Process Intensification of Mesoporous Material's Synthesis by Microwave-Assisted Surfactant Removal

López-Pérez, Lidia; López-Martínez, Marco Antonio; Djanashvili, Kristina; Góra-Marek, Kinga; Tarach, Karolina A.; Borges, María Emma; Melián-Cabrera, Ignacio

DOI
10.1021/acssuschemeng.0c05438

Publication date
2020

Document Version
Final published version

Published in
ACS Sustainable Chemistry and Engineering

ACS Sustainable Chemistry & Engineering

pubs.acs.org/journal/ascecg

Research Article

Process Intensification of Mesoporous Material's Synthesis by Microwave-Assisted Surfactant Removal

Lidia López-Pérez,[#] Marco-Antonio López-Martínez,[#] Kristina Djanashvili, Kinga Góra-Marek, Karolina A. Tarach, María Emma Borges, and Ignacio Melián-Cabrera*

Cite This: *ACS Sustainable Chem. Eng.* 2020, 8, 16814−16822

Read Online

ACCESS | Metrics & More | Article Recommendations | Supporting Information

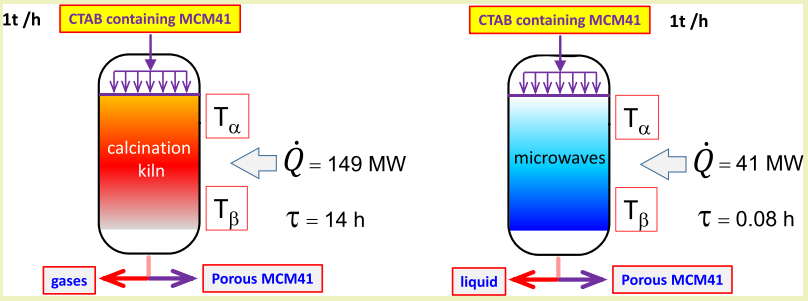

ABSTRACT: Mesoporous materials are of vital importance for use in separation, adsorption, and catalysis. The first step in their preparation consists of synthesizing an organic−inorganic hybrid in which a structuring directing agent (SDA, normally a surfactant) is used to provide the desired porosity. The most common method to eliminate the SDA, and generate the porosity, is high-temperature calcination. Such a process is energy-intensive and slow. In this study, we investigated alternative nonthermal surfactant removal methods on a soft MCM-41 material, aiming at reducing the processing time and temperature, while maximizing the material's properties. The choice of a soft MCM-41 is critical since it is hydrothermally unstable, whereas the SDA removal is troublesome. Microwave processing yielded outstanding performance in terms of surfactant removal, structural preservation, and textural features; the surfactant was fully removed, the hexagonal structure was preserved, and the surface was highly rich in Si−OH groups. It is suggested that H_2O_2 is the dominant oxidant. In terms of the process features, the processing time is significantly reduced, 14 h (calcination) *versus* 5 min (microwaves), and the applied temperature is much lower. The energy savings were estimated to be 72% lower as compared to calcination; therefore, this approach contributes to the process intensification of a very relevant material's production.

KEYWORDS: *microwave-assisted processing, structured mesoporous material, energy-saving processing, structural preservation, mild SDA removal, quick-processing, H_2O_2 oxidation*

INTRODUCTION

Mesoporous materials are highly sophisticated nanostructures with applications in catalysis, adsorption, sensing, and separation, to cite a few. They are considered as applied functional nanomaterials.[1−3] As compared to zeolites that are microporous solids (*i.e.*, pores with diameters less than 2 nm),[4] mesoporous materials expand the pore size and overcome the limitations of zeolite networks. This allows a smoother and unrestricted diffusion of bulkier molecules, and even lineal polymers can penetrate and be converted.[5] In order to obtain such a control in the pore size at nanoscale, an entirely new strategy was developed by using supramolecular organic molecules as structuring directing agents (SDA) in the sol−gel. Those templates can range from cationic, anionic, and nonionic (neutral) surfactants, normally leading to mesoporous materials,[1,6] though macroporosity can also be obtained.[7,8]

Mesoporous materials can range in the structure from hexagonal such as MCM-41 (a member of the M41S family),[9,10] SBA-15,[11,12] and SBA-3;[13] to cubic such as MCM-48,[14] FDU-5,[15] and AMS-10;[16] to caged structures such as SBA-2,[17] FDU-1,[18] SBA-1;[19] to deformed mesophases such as SBA-8[20] and KSW-2;[21] to low-order mesophases such as KIT,[22] HMS,[23] and MSU-*n*.[24] Though the composition is generally based on silica, other nonsilica compositions include alumina[25−27] or wider compositions such as CeO_2, MoO_3, WO, CeO_2−ZrO_2, αFe_2O_3, WO_3−TiO_2, and TiO_2.[28−30] The

Received: July 24, 2020
Revised: September 22, 2020
Published: October 26, 2020

https://dx.doi.org/10.1021/acssuschemeng.0c05438
ACS Sustainable Chem. Eng. 2020, 8, 16814−16822

addition of elements in smaller quantity into the main phase, for example, alumina-containing silicates, makes the spectral composition nearly infinite for mesoporous materials.

The surface and pore properties of the mesoporous materials are of great importance for applications. The first step in their manufacturing consists of obtaining the ordered nonporous organic−inorganic hybrid in which the SDA (also denoted here as surfactant) is occupying the pores. The next delicate step is to extract the surfactant from the cavities to develop the porosity, without influencing the original structure or altering the properties minimally. The SDA removal is therefore decisive on the final properties. Specifically, the SDA removal method has to be wisely adjusted as a function of the stability of the network, desired properties (*e.g.*, surface chemistry), and implementation features.

Calcination consists of a thermal treatment of the solid under air. By increasing the temperature up to 550 °C, the SDA present in the pores will decompose and finally burn out into CO_2 and H_2O. The stability upon calcination is a function of the wall thickness between the pores. However, shrinkage of the unit cell is always observed.[31] The silanol groups, $Si(OSi)_3OH$, combine to produce water, and new siloxane bonds are formed, which results in a structural shrinkage.[10,32] The formation of siloxane units can influence the surface properties, such as hydrophilicity and acidity. Hence, changes in the concentration of surface −OH groups induce variations in the surface hydrophilic/hydrophobic character. This can affect the adsorption of reagents both in the number of adducts formed and their nature. In order to minimize the calcination side effects, different approaches have been suggested.[33−35] However, controlling the surface chemistry is still a challenging target.

Mesoporous materials of high interest are those that are synthesized in simple manners, which often implies free of hydrothermal treatment.[36] However, the drawback is that these structures are soft and prone to damage in successive processing steps. The primary goal of this work was to identify a suitable method to remove the SDA of a soft MCM-41 material, aiming at a process that reduces the processing time and decreases the energy consumption, and the material's properties are maximized. Therefore, we were looking at an intensified process for mild nonthermal SDA removal of a relevant MCM-41 material. The methodology reported by Tian *et al.*[37] using microwaves is attractive, which was applied on SBA-15. However, applying such a methodology onto MCM-41 is not a rational choice since the materials' hydrothermal stability is very different; SBA-15 is hydrothermally stable, whereas the studied MCM-41 is not. Therefore, this work provides more value to the microwave processing since it expands its application range to hydrothermally unstable materials. Most importantly, this work provides original aspects from the process point of view, in terms of significant energy reduction through the microwave processing.

EXPERIMENTAL SECTION

Chemicals. The employed chemicals are summarized in Table S1 (Supporting Information).

Synthesis of the Mesophase. The MCM-41 mesophase was prepared at room temperature following the procedure reported by Grün *et al.*[36] A solution containing the quaternary ammonium salt [cetrimonium bromide (CTAB), as the SDA] in Milli-Q water was prepared under gentle magnetic stirring. Aqueous ammonia was added to the solution as a catalyst. Then, tetraethyl orthosilicate (TEOS) was added dropwise. During the addition of TEOS, the mixture began to whiten resulting in a gel with the following molar composition: 1 TEOS/0.152 CTAB/2.8 NH_3/141.2 H_2O. The mixture was stirred for 1 h. The precipitate was recovered by suction filtration and washed with abundant water. A fine white powder was obtained after drying overnight at 90 °C. Note that the terms SDA and surfactant are equally used along the manuscript; they are equivalent terms.

SDA Removal Methodologies. *Calcination.* A ceramic cup, which contained the sample, was placed in the center of a box Nabertherm furnace, equipped with a P330 temperature controller, and heated from room temperature up to 550 °C for 5 h in the presence of static air. The heating rate was 1 °C/min.

Solvent Extraction. The method consisted of contacting the solid with an acidic ethanol solution at the reflux temperature. One gram of the mesophase was contacted with 300 mL of a 1.0 M HCl solution in ethanol. The mixture was stirred and kept in reflux for 30 h at the reflux temperature (~78 °C). The sample was filtered and washed with abundant water and dried in an oven at 110 °C.

Ozonation. The treatment with ozone was performed according to the procedure reported by Büchel *et al.*[38] The method consists of bubbling *in situ* produced ozone through a mixture of the material and water. Typically, 1 g of the precursor material was contacted with 150 mL of Milli-Q water and agitated with a magnetic stirrer. Ozone was then introduced to the slurry by bubbling the gas through a glass tube. At the beginning of the reaction, the hydrophobic powder (mesophase containing the template) did not mix well in water and remained on top of the liquid surface. After approx. 30 min, the slurry resulted in a homogeneous suspension. The experiment was stopped after 8 h; the slurry was filtered, washed with abundant water by filtration, and dried in an oven at 110 °C.

Microwave-Assisted Template Removal. A microwave sample preparation system MDS 2000 (CEM Corporation) was used, equipped with Teflon sample vessels transparent for microwave radiation. The working frequency and voltage of the equipment were 2450 MHz and 220 V, respectively. The samples were prepared in the Teflon vessel using 0.15 g of mesophase combined with 1.5 mL of HNO_3 solution and 1.0 mL of H_2O_2 (see concentrations in the Supporting Information, Table S1) using a modified protocol, as reported elsewhere.[37] The maximum observed temperature was 200 °C. The mesophase was first exposed to different treatment times to determine the time needed to fully remove the template. Preliminary experiments were performed for 3, 5, and 7 min. A processing time of 5 min was found to be necessary to achieve full SDA removal. The slurry was filtered, washed with abundant water by filtration, and dried in an oven at 110 °C.

Fenton-Assisted SDA Removal. The procedure was carried out following the protocol described by López Pérez *et al.*[10] in the liquid phase without the need of any solvent.

Characterization Methods. *Elemental Analysis.* CHN elemental analysis was carried out on a EuroVector 3000 CHNS analyzer using approximately 2 mg sample, which was weighted on a 6-digit Mettler-Toledo analytical scale. The analyses were performed in duplicate, and only analyses with a 2% standard deviation were employed. The analysis itself consists of burning the samples at 1700−1800 °C in the presence of an oxidation catalyst. The organics are decomposed into CO_2, H_2O, SO_2, and N_2 and then separated *via* an online gas chromatograph having a Poropak QS column, operated isothermally at 80 °C, and quantified with a thermal conductivity detector. Calladius software was used to obtain the quantitative information. The integrated peak area was converted into a percentage using acetanilide (99.9%) as an external standard.

Structure. The structural ordering was evaluated by small-angle X-ray scattering (SAXS) on a Bruker NanoStar instrument, containing a ceramic fine-focus X-ray tube, which was powered by a Kristallflex K760 generator at 35 kV and 40 mA. The X-ray flux was collimated using cross-coupled Göbel mirrors and a 0.1 mm diameter pinhole, providing a Cu Kα beam with a full width at half-maximum of about 0.2 mm at the sample position. The sample-to-detector distance was

https://dx.doi.org/10.1021/acssuschemeng.0c05438
ACS Sustainable Chem. Eng. 2020, 8, 16814−16822

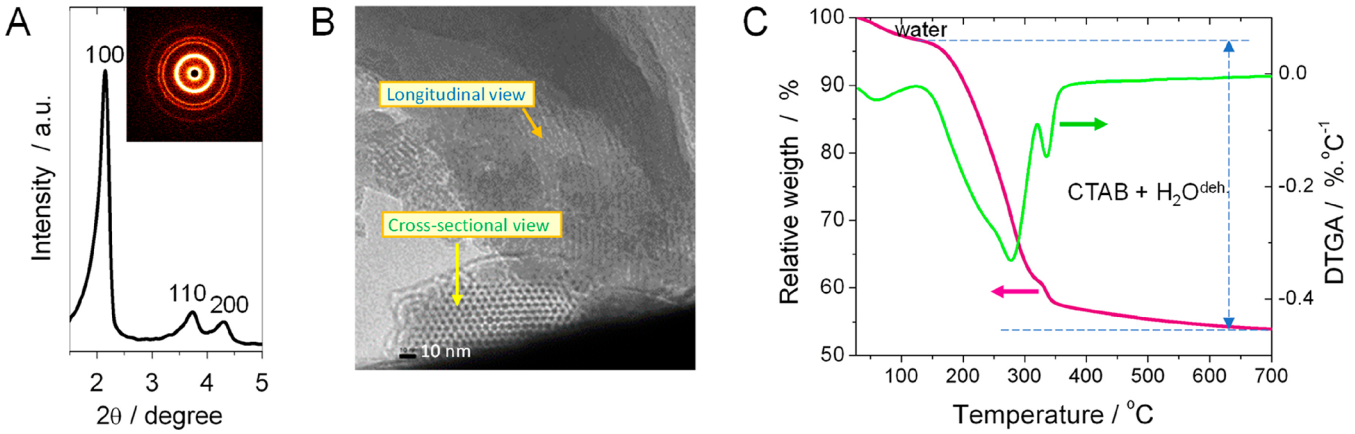

Figure 1. MCM-41 mesophase. (A) SAXS (inset: measured 2D scattering pattern), (B) HRTEM, and (C) TGA/DTGA analyses. In (C) CTAB + H_2O^{deh} means that the weight loss is due to the combustion of the CTAB plus the water coming from the dehydroxylation of the material (2Si−OH → Si−O−Si + H_2O), *i.e.*, the reason we employed CHN elemental analysis as it is an element-selective technique.

1.04 m. The scattering intensity was registered by a Siemens AXS Hi-Star detector in the q-vector range of 0.1−2.0 nm.

Gas Adsorption. Nitrogen adsorption isotherms at −196 °C were obtained on a QuantaChrome Autosorb-6B apparatus. The materials were previously evacuated at 150 °C for 16 h. The Brunauer−Emmett−Teller (BET) method was used to calculate the surface area (S_{BET}) of the samples. The Barrett−Joyner−Halenda (BJH) method was applied for deriving the pore size distributions (PSDs) of the solids. The total pore volume was estimated from the adsorbed amount at a relative pressure of 0.98 in the desorption branch.

Thermal Analysis. Thermogravimetric analyses (TGAs) were carried out in a TGA/SDTA851e Mettler-Toledo analyzer, where around 5 to 10 mg of the sample was loaded into a 70 μL α-Al_2O_3 crucible. The temperature was raised from 30 to 900 °C at a rate of 10 °C/min under a flow of synthetic air (100 mL/min). Baseline subtraction was employed to remove geometrical and crucible effects in the pattern. Differential TGA (DTGA) was obtained from the instrument software.

Scanning Electron Imaging. Scanning electron microscopy (SEM) images were recorded with a Philips XL 20 microscope at 10 kV. Samples were coated with gold to improve contrast.

High-Resolution Transmission Electron Imaging. Transmission electron microscopy (TEM) micrographs were recorded on a JEOL 2010. A small amount of the sample was grinded with a mortar and pestle and dispersed in isopropanol. A small drop was dispersed on a Holey carbon grid (TED Pella 300 copper mesh) and left to dry. Images were taken at 200 kV in brightfield and analyzed using the software Gatan Digital Micrograph.

DRIFT Spectra. The IR spectra of the materials were collected on a Nicolet Magna 860 spectrometer, equipped with a DTGS (deuterated triglycine sulfate) detector and a Praying Mantis Harrick DRIFT cell. The spectra were acquired by co-addition of 256 scans with a resolution of 4 cm^{-1}. About 50 mg of the pure material was packed into a sample holder, synthetic air was passed over the sample, and the material was mildly dried at 150 °C until the baseline of the m/z = 18 (H_2O) of the outlet gas stream went to a baseline level, indicating that the physisorbed water was removed from the sample's surface. A diffuse reflectance Fourier transform (DRIFT) spectrum of dried KBr (Aldrich, FTIR grade) was first recorded as a background.

Solid-State NMR. ^{29}Si MAS NMR spectra were measured on a Varian VXR-400S spectrometer at 79.44 MHz using a 7 mm zirconium spinner, with the following settings: spinning speed 5 KHz, acquisition time 0.2 s, acquisition delay 20 s, radiofrequency length 3.2 μs, spectral window 30,007 Hz, and 3200 scans. Tetramethylsilane was used as a reference.

RESULTS AND DISCUSSION

Mesophase. The mesophase was prepared according to the study of Grün *et al.*[36] SAXS analysis reveals a mesophase having well-defined hexagonally packed cylindrical morphology characterized by a distance between the cylinders of 4.76 nm (Figure 1A), which was confirmed by high-resolution TEM (HRTEM) (Figure 1B). SEM provided information on the particle morphology, displaying agglomerates of particles that are mostly unconnected of relatively small size, ∼0.5 × 2 μm (Figure S1 in the Supporting Information). TGA (Figure 1C) indicates that the mesophase requires a thermal treatment of 550 °C to decompose the SDA (*i.e.*, CTAB surfactant). The surfactant is present in 42 wt % and decomposes in two steps, in agreement with prior studies, DTGA, as shown in Figure 1C.[39,40]

Calcination. As discussed earlier in the background, calcination may produce a structural shrinkage. This is shown in Figure 2A, where the main (100) reflection shifts to higher angles. The hexagonal a_0 lattice parameter changes from 4.76 to 4.28 nm, representing 10% contraction. The

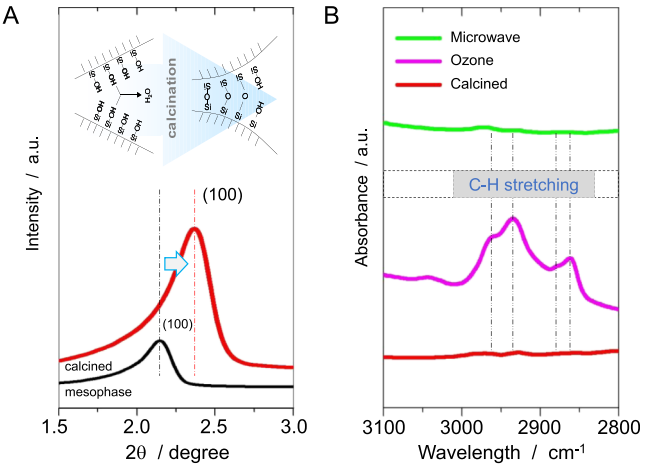

Figure 2. (A) SAXS patterns in the (001) region of the mesophase and calcined counterpart. Inset: representation of the structural shrinkage upon calcination. Silanol groups combine, and siloxane bonds are formed, resulting in structural shrinkage with a loss of pore volume. (B) DRIFT spectra of the C−H region for three relevant materials.

https://dx.doi.org/10.1021/acssuschemeng.0c05438
ACS Sustainable Chem. Eng. 2020, 8, 16814−16822

contraction of the structure is not a big problem for catalysis purposes, but the main drawback of calcination refers to the fact that it irreversibly reduces the density of surface OH groups and, from the practical point of view, it is a slow and an energy-intensive process.

Nonthermal SDA Removal Methodologies. After performing mild SDA removal protocols on the mesophase, the resulting materials were characterized by several techniques to assess template removal and the materials' properties.

Surfactant Removal Efficiency. TGA gave ambiguous information as the mildly treated materials have a significant weight loss due to dehydroxylation's water release (see note in Figure 1's caption). CHN analysis is, however, selective and can provide a straight account of the SDA removal. Therefore, the template removal efficiency was obtained after comparing the elemental composition (CHN analysis) before and after each procedure (Table 1). Besides calcination that removes entirely the SDA, microwave oxidation and Fenton are the most effective alternatives to calcination. High SDA removal was also obtained by solvent extraction. Ozonation does not provide good results with an SDA removal efficiency of 29% only. These results were compared with the DRIFT spectra (Figure 2B). Inspection of the 2840−3000 cm^{-1} C−H region confirms that the SDA removal is complete for the microwaved material, being as efficient as calcination. As a reference case, the ozone treatment shows a substantial contribution of C−H groups originating from the undecomposed SDA.

Table 1. MCM-41 Materials' Properties after Applying Various SDA Removal Methodologies

material	SDA removal (%)[a]	a_0 (nm)[b]	S_{BET} (m^2/g)	V_{total} (cm^3/g)
mesophase (untreated)	0 (reference)	4.76	21	0.04
calcination	100	4.28	1077	0.85
solvent extraction	97	Am[c]	456	0.25
ozone	29	4.57	545	0.31
microwaves	99	4.49	923	0.82
Fenton	98	4.68	636	0.37

[a]SDA removal calculated as: η (%) = $(1 - C^{material}/C^{mesophase}) \times 100$, where $C^{material}$ is the carbon concentration of the material and $C^{mesophase}$ is the carbon concentration of the mesophase; the raw data (wt % C) can be found in the Supporting Information (Table S2). [b]a_0 = the lattice parameter, from the SAXS pattern: $a_0 = (2/\sqrt{3})\cdot d_{100}$. [c]Fully amorphous.

Structural Ordering. Small-angle X-ray diffraction patterns provide information about the structural changes upon each SDA removal strategy (Figure 3A). Structural shrinkage is detected for all (100)-displaying materials. The main Bragg diffraction peak (100) is shifted to higher values that results in smaller cell parameters (a_0, Table 1). The larger degree of shrinkage took place upon calcination (∼10%). Shrinkage was also observed upon microwave oxidation (∼6%). The temperatures achieved during microwave radiation (∼200 °C) and the presence of H_3O^+ ($H_5O_2^+$) in an aqueous environment may explain the structural shrinkage. Such a shrinkage was also found, but to a lower extent, in the ozonation and Fenton treatments (4 and 2%, respectively). The reason for shrinkage in these cases appears to be related to hydrolysis of the soft uncalcined silica framework. This is supported by the conclusions of López Pérez *et al.*,[10] who showed that a 70 °C-Fenton treatment leads to severe structural collapse on an MCM-41 mesophase. This was explained by the high capillary forces during the drying of the pores; similar observations were found for SBA-15, associated to the soft nature of the silica network as well.[12]

Changes in the mesoscopic ordering were observed by comparing the SAXS patterns, as shown in Figure 3A. Calcination shows the highest degree of ordering, followed by microwaving with a less intense and broader (100)

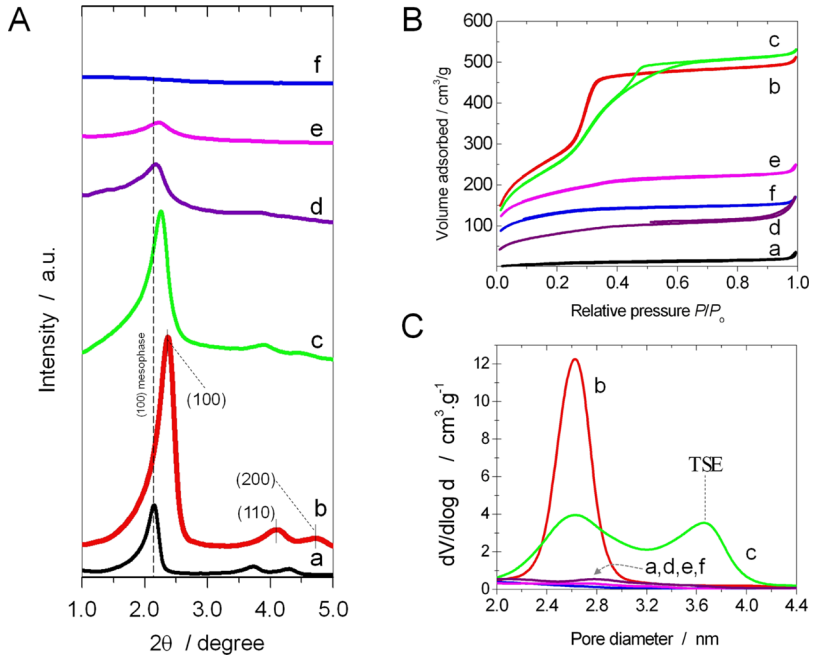

Figure 3. Effect of the SDA removal methodologies on MCM-41. (A) SAXS patterns. (B) N_2 adsorption isotherms. (C) BJH pore size distribution. Materials: (a) untreated mesophase, (b) calcination, (c) microwaves, (d) Fenton chemistry, (e) ozonation, and (f) solvent extraction. Isotherms in (B) were offset for clarity.

https://dx.doi.org/10.1021/acssuschemeng.0c05438
ACS Sustainable Chem. Eng. 2020, 8, 16814−16822

reflection. The second-order reflections of this material are also less intense; hence, the material's contraction is isotropic (*i.e.*, $x \sim y \sim z$). The Fenton treatment only presented an ill-defined (100) peak, while the secondary ones were undetected. The structures with the lowest ordering correspond to the ozone treatment followed by the solvent extraction; in the latter case, no pattern was detected. The materials which were exposed to an aqueous environment for prolonged periods of time resulted in structural collapse, most likely due to hydrolysis. Control tests were carried out to verify that hypothesis. The calcined MCM-41 was hydrothermally treated at 70 °C mirroring those treatments. From these experiments, it became evident that the hydrothermal treatment leads to severe structural and textural modifications, as evidenced from SAXS patterns (Figure 4A) and isotherms (Figure 4B, textural parameters can be found in Table S3 in the Supporting Information). Even after 1 h, the structure fully collapses with a severe drop in the textural parameters (Table S3 in the Supporting Information). These results confirm the susceptibility of this mesophase toward hydrothermal treatments due to hydrolysis.

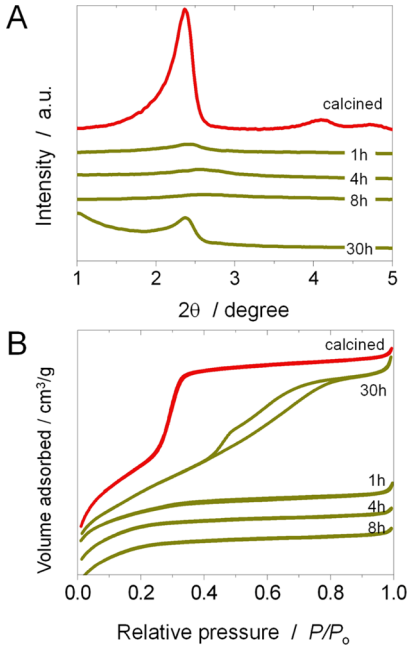

Figure 4. Stability of MCM-41 after hydrothermal treatment at 70 °C. (A) Evolution of the structural changes by SAXS, treatment time is indicated. (B) Nitrogen sorption isotherms of the corresponding materials.

Textural Features. The textural properties were studied by gas adsorption. The nitrogen isotherms (Figure 3B) show type IV isotherms for the calcined and microwave-processed materials. Calcination of the mesophase gives rise to a well-defined porosity with a fully reversible adsorption isotherm. It has a specific surface area of 1077 m^2/g and a pore volume of 0.85 cm^3/g. The porosity of the other materials is affected by alterations and/or damage in the structure. The microwaved material is the one which still shows a high adsorption capacity with a moderate modification in the pore-filling mechanism. It is not as sharp as in the calcined case, and it occurs in two steps. The other materials do not show a steep pore-filling step, but it is nearly flat in the typical mesopore region; they possess lower surface areas and pore volumes (Table 1).

The BJH PSDs (Figure 3C) are in agreement with the SAXS ordering. Only the calcined material has a well-resolved BJH PSD at around 2.6 nm. The microwaved material has a broader pattern with the prevalence of pore sizes at *ca.* 2.6 nm. The pore maximum at high P/P_0 is due to a phenomenon called tensile strength effect (TSE) (Figure 3C).[41] Despite having the TSE effect, the PSD of the microwaved material shows evidence of having broader pores; this was verified by estimating the average pore size as $4 \times 10^3 \times V_{total}/S_{BET}$, which resulted in 3.2 nm for the calcined and 3.6 nm for the microwaved one. Note that it is known that the BJH model gives an underestimation of the pore size when comparing BJH with geometrical pore size values.[42] The other materials displayed a PSD with a baseline-like pattern. Despite the microwave approach modified the PSD with secondary larger pores, this did not have a big effect in the textural parameters. The BET surface area and pore volume remain high with 923 m^2/g and a pore volume of 0.82 cm^3/g. This is 85 and 96% of the BET and pore volume retention, respectively, as compared to calcination. The drop in the BET surface area is due to having bigger pores.

The broader PSD of the microwaved material was further investigated by HRTEM (Figure 5A). It was found that the material was in general ordered but some domains were more amorphous, indicating the disturbance of the regularity. This is ascribed to hydrolysis, which makes the structure more disordered. The combination of water and local hot-spots, originated from the microwave beam, can alter local parts of

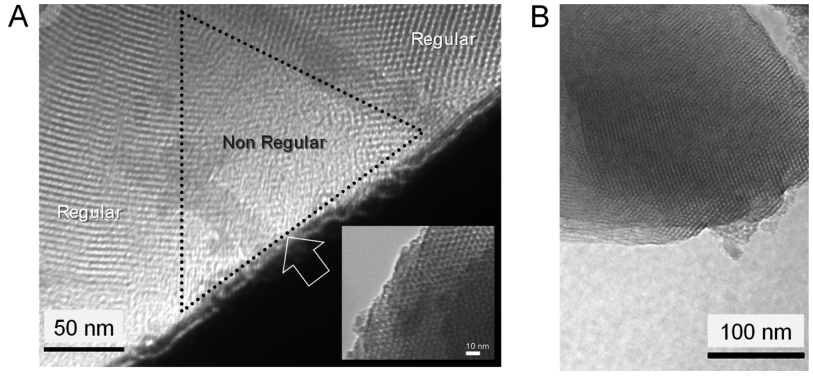

Figure 5. (A) HRTEM of the microwaved-processed structure showing areas with damage associated to hydrolysis (highlighted with the arrow). The inset shows a front view of the pores having a well-defined hexagonal symmetry. (B) HRTEM of the calcined material.

https://dx.doi.org/10.1021/acssuschemeng.0c05438
ACS Sustainable Chem. Eng. 2020, 8, 16814−16822

the material. Such an effect was absent in the calcined material (Figure 5B) where a regular distribution of pores/channels was observed across the particle.

To understand better the PSD broadening, one must bear in mind that the microwave processing functions like a batch autoclave where the pressure increases above 1 MPa and temperature peaks at around 200 °C. That means that such a treatment can act as a secondary hydrothermal step on the structure. It was generally found for SBA-15 materials that the pore size increases with the hydrothermal temperature during the hydrothermal ageing;[33] a similar effect may be occurring here where the pore size is expanded due to the microwave-induced heat and autogenous pressure. However, it is not yet entirely clear whether the effect in this situation is local or not (*i.e.*, affecting the whole sample or a section) since the TEM images did not have enough resolution in the range of the observed pore sizes, 2−4 nm, to identify the pore broadening. In practical terms, the pore expansion may be resolved, or minimized, by novel reactor concepts with controlled doses of microwaves, spinning, and so forth, as will be outlined later. Therefore, this approach can still be considered as suboptimal at this stage.

Silanol Characterization. The properties of the resulting material in terms of the silanol groups were studied by DRIFT and ^{29}Si MAS NMR. Several kinds of silanol groups can be distinguished in the IR spectra (Figure 6A). Freely oscillating

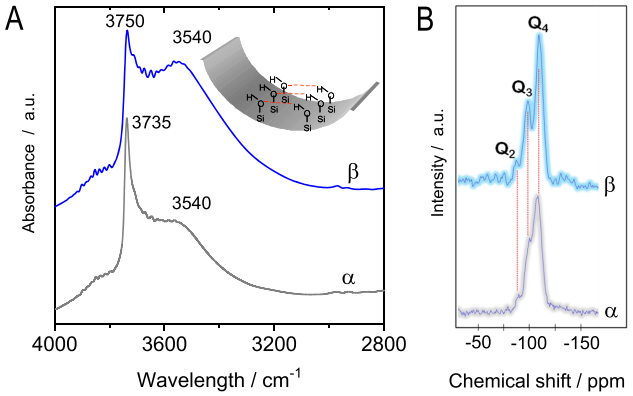

Figure 6. (A) DRIFT spectra analysis of the O−H region; the inset represents a highly hydroxylated surface in the microwaved material's surface. (B) ^{29}Si MAS NMR spectra. Materials: (α) calcined and (β) microwaved-processed materials.

isolated terminal $(SiO)_3Si-OH$ were found at 3750 cm^{-1}. The broad band at 3540 cm^{-1} is typical of strongly linked silanols as vicinal hydrogen-bonded silanols (dimers or higher).[43] It is well seen that the microwaved treatment results in a *ca.* two-fold higher number of hydrogen-bonded silanols (higher intensity of the 3540 cm^{-1} band). This suggests that the microwave treatment does not condense the silanols as calcination does, and it may contain surface defects where the OH-linked silanols are located. The concentration of the hydrogen-bonded silanols normally decreases by increasing the pore size,[44] but this is not observed for the microwaved material despite having broader pores, which is a positive feature.

^{29}Si MAS NMR completes the interpretation of the surface chemistry (Figure 6B). The Q_2 [$Si(OSi)_2(HO)_2$, geminal] and Q_3 [$Si(OSi)_3(HO)$, isolated and vicinal terminal] are more pronounced in the microwaved material. This corresponds to the presence of a highly hydroxylated surface. The concentration of Si−OH was quantified (Table 2), resulting in

Table 2. Quantification of the ^{29}Si MAS NMR Q_n Species and Si−OH Concentration

material	Q_2 (%)	Q_3 (%)	Q_4 (%)	Si−OH(%)[a]
mesophase (untreated)	0.5	37.7	61.8	38.7 (100)
calcination	0.7	30.1	69.2	31.5 (81)
microwaves	2.1	33.4	64.5	37.6 (97)

[a]Si−OH (%) = $[(2Q_2 + Q_3)/\sum Q_i] \times 100$. [b]Values between parenthesis correspond to the percentage of retention of the Si−OH using the parent mesophase as a reference (*i.e.*, 100%).

comparable values between the microwave-processed MCM-41 and the starting mesophase, whereas the calcined counterpart lost 19%. The high Si−OH in the microwaved material has to do with the mild conditions; there is no thermal condensation of Si−OH into siloxane. This explains that the mesophase and the microwave-processed materials have a comparable Si−OH concentration. The highly hydroxylated surface's nature of the microwaved material can also be seen in the Q_4 ($Si(OSi)_4$) NMR's peak. The upfield shift of the resonance toward the negative edge suggests the removal of a less electronegative element from the Si local environment. This indicates the engagement of H from an OH group in the hydrogen bond with a neighboring O-atom from the silanols.

In practical terms, having a high amount of silanols (not Si−O−Si units) makes the microwave-processed material more hydrophilic, opening doors of adsorption strategies for improved drug load,[45] or grafting procedures where the high concentration of silanols would be needed. Figure 6A (inset) represents a section of the pore displaying a high density of Si−OH; in this case, for simplicity, the vicinal ones have been represented.

Mechanistic Considerations for the Microwave-Processing Method. When comparing the oxidation potentials between the two employed oxidants, it is thought that the prevalent oxidizing agent is H_2O_2 (1.776 V)[46] while HNO_3 (0.803−0.934 V)[46] can only have an acidifying role. This opens up the possibility to optimize the process by reducing the use of HNO_3 in a successive study. Though Fenton radicals (2.800 V)[47] are stronger in terms of oxidation potential than H_2O_2, the benefit of the microwaves is the fact that the temperature increases up to 200 °C; this favors the SDA oxidation kinetics using H_2O_2. Under ambient conditions, Fenton chemistry would be better since the maximum temperature is given by the H_2O_2/H_2O mixture's boiling temperature, *ca.* 100 °C; at these conditions, H_2O_2 cannot compete in kinetic terms with Fenton chemistry. However, as seen in the material properties, Fenton does not work well for this material since it leads to severe structural and textural collapse. In other words, the microwave-induced autoclaving effect promotes the oxidation kinetics of H_2O_2 and makes it an effective oxidant for CTAB oxidation. A tentative mechanism for the SDA removal can be defined as, eq 1

$$SiO_x(OH)_{2-x}(CTAB) + \alpha H_2O_2 \xrightarrow{H^+} SiO_x(OH)_{2-x}(\ ) + \beta CO_2 + \gamma H_2O + \delta HBr/Br_2 + \varepsilon NO \quad (1)$$

https://dx.doi.org/10.1021/acssuschemeng.0c05438
ACS Sustainable Chem. Eng. 2020, 8, 16814−16822

where CTAB is decomposed into CO_2, H_2O, HBr/Br_2, and NO. $SiO_x(OH)_{2-x}(\ )$ represents the SDA-free MCM-41 material, containing siloxanes and silanols.

Methodologies' Evaluation. It is outstanding that the majority of materials underwent structural damage upon different SDA removal methodologies. This supports the fact that the mesophase, without hydrothermal treatment, does not have an adequate hydrothermal stability. The success of the microwave treatment in keeping the structure is associated to the short treatment times (minutes); this enables the SDA removal and minimizes the structural damage.

A comparison of the protocols' properties is given in Table 3. Most of the methodologies are effective in removing the SDA (rated as ++) except ozonation (+). The SDA removal approach utterly affects the ordering leading to less ordered (+/−) or amorphous (−) structures, with the exception of calcination (++) and microwave treatment (+). The ordering is directly linked to the porosity; those materials with higher ordering display better textural parameters. The evaluation also considers process features. Calcination is slow due to the low heating rates, with a total processing time of ∼14 h. The corrosive gases can affect irreversibly the calcination equipment, leading to a long return on investment (*i.e.*, recapitalization), and it is highly energy-intensive process. Microwave is a much faster protocol and operates at a lower temperature. The Fenton chemistry-derived material would be improved by drying using a low-surface tension solvent, as proven by López Pérez *et al.*,[10] in the sense that the structure was much better preserved when H_2O was replaced by *n*-BuOH during the drying. This avoids surface tension-induced collapse. However, such *n*-BuOH post-treatment notably increases the complexity of the work-up, whereas the microwave processing seems to overcome such problems in a simpler way using low-cost chemicals in a quick manner.

Table 3. Comparison of the Various SDA Removal Methodologies

	material's features		
methodology	SDA removal	ordering	porosity
calcination	++	++	++
solvent extraction	++	−	<500 m^2/g, flat PSD
ozone	+	−	<600 m^2/g, flat PSD
microwaves	++	+	++ with some pore expansion
Fenton	++	+/−	<650 m^2/g, flat PSD

From the energy consumption view point, the microwave processing has benefits with a lower carbon footprint. Figure 7 compares the energy required to process a feedstock of 1 t/h of a CTAB-containing MCM-41 between calcination and microwaves. The calculation renders a reduction of the energy consumption by 72% from 149 to 41 MW. Therefore, both rapidness and energy reduction contribute to a more intensified process. These results are in line with recent studies that have shown the benefit of microwave-assisted processing for reactor operation under selective heating at both macro and microscale, whereas conventional conduction heating is nonselective by itself or less efficient.[48−50]

CONCLUSIONS

A rapidly synthesized soft MCM-41 material was subjected to state-of-the-art thermal and nonthermal SDA removal methods. Certain methods promoted severe hydrolysis and provoked significant changes of the structure. Microwave-assisted processing was effective and quick in removing the SDA/surfactant, and it yielded a different material than that obtained by calcination. The hexagonal structure was preserved, and broader pores were found, in addition to the main ones; this was ascribed to some degree of hydrolysis, in combination with the hydrothermal conditions during the microwave processing, but did not affect the total surface area which was high. The surface of the material is highly rich in Si−OH, with a great promise for further use. The benefits of the microwaves from the process point of view, as compared to calcination, are the short processing time, that it is reduced from 14 h (calcination) into 5 min (microwaves) and the lower applied temperature. The latter has an impact with a reduction by 72% of the carbon footprint. This makes it appealing for further applications to other materials or other approaches, not necessarily oxidations but extractions.

ASSOCIATED CONTENT

Supporting Information

The Supporting Information is available free of charge at https://pubs.acs.org/doi/10.1021/acssuschemeng.0c05438.

Chemicals employed for the synthesis and postsynthesis processing steps; elemental analyses of the processed materials; textural parameters of the processed materials (BET surface area, total pore volume, pore diameter, and external surface area); SEM image of the synthesized mesophase; and theoretical background for the energy balance calculation (PDF)

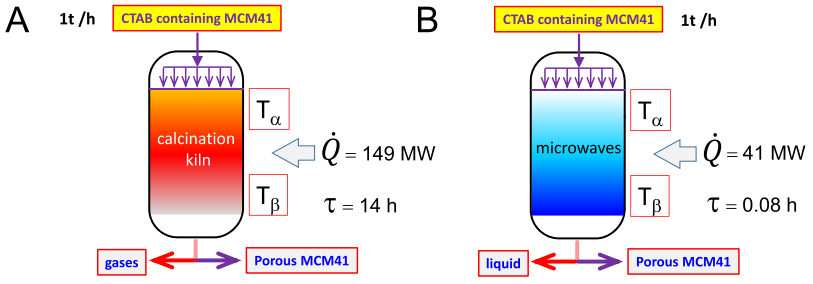

Figure 7. Reactor models representing calcination (A) and the microwaves processing (B) of a solid feedstock of 1 t/h of CTAB-containing MCM-41. The methodology can be found in the Supporting Information.

https://dx.doi.org/10.1021/acssuschemeng.0c05438
ACS Sustainable Chem. Eng. 2020, 8, 16814−16822

AUTHOR INFORMATION

Corresponding Author

Ignacio Melián-Cabrera − *Chemical Engineering Department, School of Engineering and Technology, University of La Laguna, 38200 San Cristóbal de La Laguna, S/C de Tenerife, Spain;* orcid.org/0000-0002-5132-6743; Email: ignacio.melian.cabrera@ull.edu.es

Authors

Lidia López-Pérez − *Faculty of Science and Engineering, University of Groningen, 9747 AG Groningen, The Netherlands; División de Ciencias Básicas e Ingeniería, Universidad Autónoma Metropolitana-Unidad Azcapotzalco, 02200 Mexico City, Mexico;* orcid.org/0000-0001-5587-4467

Marco-Antonio López-Martínez − *División de Ciencias Básicas e Ingeniería, Universidad Autónoma Metropolitana-Unidad Azcapotzalco, 02200 Mexico City, Mexico*

Kristina Djanashvili − *Department of Biotechnology, Delft University of Technology, 2629HZ Delft, The Netherlands;* orcid.org/0000-0003-1511-015X

Kinga Góra-Marek − *Faculty of Chemistry, Jagiellonian University in Kraków, 30-387 Kraków, Poland;* orcid.org/0000-0002-1296-9244

Karolina A. Tarach − *Faculty of Chemistry, Jagiellonian University in Kraków, 30-387 Kraków, Poland;* orcid.org/0000-0003-0133-4363

María Emma Borges − *Chemical Engineering Department, School of Engineering and Technology, University of La Laguna, 38200 San Cristóbal de La Laguna, S/C de Tenerife, Spain*

Complete contact information is available at: https://pubs.acs.org/10.1021/acssuschemeng.0c05438

Author Contributions

#L.L.-P. and M.-A.L.-M. contributed equally.

Notes

The authors declare no competing financial interest.

ACKNOWLEDGMENTS

De Nederlandse Organisatie voor Wetenschappelijk Onderzoek (NWO, The Netherlands) is thanked for the financial support of the VIDI (project no. 10284). L.L.P. thanks the UAM for grant number 22301055 (programa especial de la Dirección de Apoyo a la Investigación). O. Rojas and G. ten Brink (RUG) are thanked for assistance on the TEM images and preliminary results.

REFERENCES

(1) Zhao, D. Y.; Wan, Y.; Zhou, W. *Ordered Mesoporous Materials*; Wiley-VCH: Weinheim, 2013.

(2) Wang, Y.; Du, X.; Liu, Z.; Shi, S.; Lv, H. Dendritic fibrous nanoparticles (DFNPs): rising stars of mesoporous materials. *J. Mater. Chem. A* **2019**, *7*, 5111−5152.

(3) Wu, K. C.-W.; Jiang, X.; Yamauchi, Y. New trend on mesoporous films: precise controls of one-dimensional (1D) mesochannels toward innovative applications. *J. Mater. Chem.* **2011**, *21*, 8934−8939.

(4) IUPAC Gold Book. URL: https://goldbook.iupac.org/terms/view/M03906 (accessed July 20, 2020).

(5) Parlett, C. M. A.; Wilson, K.; Lee, A. F. Hierarchical porous materials: catalytic applications. *Chem. Soc. Rev.* **2013**, *42*, 3876−3893.

(6) Zhao, D. Y. In *Introduction to Zeolite Science and Practice*, 3rd revised ed.; Cejka, J.; van Bekkum, H.; Corma, A.; Schüth, F. ., Eds.; Elsevier B.V.: Amsterdam, 2007; Vol. *168*, pp 241−300.

(7) Imhof, A.; Pine, D. J. Ordered macroporous materials by emulsion templating. *Nature* **1997**, *389*, 948−951.

(8) Parlett, C. M. A.; Isaacs, M. A.; Beaumont, S. K.; Bingham, L. M.; Hondow, N. S.; Wilson, K.; Lee, A. F. Spatially orthogonal chemical functionalization of a hierarchical pore network for catalytic cascade reactions. *Nat. Mater.* **2016**, *15*, 178−182.

(9) Kresge, C. T.; Leonowicz, M. E.; Roth, W. J.; Vartuli, J. C.; Beck, J. S. Ordered mesoporous molecular sieves synthesized by a liquid-crystal template mechanism. *Nature* **1992**, *359*, 710−712.

(10) López Pérez, L.; Ortiz-Iniesta, M. J.; Zhang, Z.; Agirrezabal-Telleria, I.; Santes, M.; Heeres, H. J.; Melián-Cabrera, I. Detemplation of soft mesoporous silicana nanoparticles with structural preservation. *J. Mater. Chem. A* **2013**, *1*, 4747−4753.

(11) Zhao, D.; Feng, J.; Huo, Q.; Melosh, N.; Fredrickson, G. H.; Chmelka, B. F.; Stucky, G. D. Triblock copolymer syntheses of mesoporous silica with periodic 50 to 300 angstrom pores. *Science* **1998**, *279*, 548−552.

(12) Zhang, Z.; Melián-Cabrera, I. Modifying the hierarchical porosity of SBA-15 via mild-detemplation followed by secondary treatments. *J. Phys. Chem. C* **2014**, *118*, 28689−28698.

(13) Huo, Q.; Margolese, D. I.; Ciesla, U.; Feng, P.; Gier, T. E.; Sieger, P.; Leon, R.; Petroff, P. M.; Schüth, F.; Stucky, G. D. Generalized synthesis of periodic surfactant/inorganic composite materials. *Nature* **1994**, *368*, 317−321.

(14) Alfredsson, V.; Anderson, M. W. Structure of MCM-48 revealed by transmission electron microscopy. *Chem. Mater.* **1996**, *8*, 1141−1146.

(15) Liu, X.; Tian, B.; Yu, C.; Gao, F.; Xie, S.; Tu, B.; Che, R.; Peng, L.-M.; Zhao, D. Room-temperature synthesis in acidic media of large-pore three-dimensional bicontinuous mesoporous silica with *Ia3d* symmetry. *Angew. Chem., Int. Ed.* **2002**, *41*, 3876−3878.

(16) Gao, C.; Sakamoto, Y.; Sakamoto, K.; Terasaki, O.; Che, S. Synthesis and characterization of mesoporous silica AMS-10 with bicontinuous cubic Pn_3m symmetry. *Angew. Chem., Int. Ed.* **2006**, *45*, 4295−4298.

(17) Huo, Q.; Leon, R.; Petroff, P. M.; Stucky, G. D. Mesostructure design with gemini surfactants: supercage formation in a three-dimensional hexagonal array. *Science* **1995**, *268*, 1324−1327.

(18) Yu, C.; Yu, Y.; Miao, L.; Zhao, D. Highly ordered mesoporous silica structures templated by poly(butylene oxide) segment di- and tri-block copolymers. *Microporous Mesoporous Mater.* **2001**, *44*−*45*, 65−72.

(19) Zhao, D.; Huo, Q.; Feng, J.; Kim, J.; Han, Y.; Stucky, G. D. Novel mesoporous silicates with two-dimensional mesostructure direction using rigid bolaform surfactants. *Chem. Mater.* **1999**, *11*, 2668−2672.

(20) Kimura, T.; Kamata, T.; Fuziwara, M.; Takano, Y.; Kaneda, M.; Sakamoto, Y.; Terasaki, O.; Sugahara, Y.; Kuroda, K. Formation of novel ordered mesoporous silicas with square channels and their direct observation by transmission electron microscopy. *Angew. Chem., Int. Ed.* **2000**, *39*, 3855−3859.

(21) Ryoo, R.; Kim, J. M.; Ko, C. H.; Shin, C. H. Disordered molecular sieve with branched mesoporous channel network. *J. Phys. Chem.* **1996**, *100*, 17718−17721.

(22) Tanev, P. T.; Pinnavaia, T. J. Mesoporous silica molecular sieves prepared by ionic and neutral surfactant templating: a comparison of physical properties. *Chem. Mater.* **1996**, *8*, 2068−2079.

(23) Kleitz, F.; Liu, D.; Anilkumar, G. M.; Park, I.-S.; Solovyov, L. A.; Shmakov, A. N.; Ryoo, R. Large cage face-centered-Cubic *Fm3m* mesoporous silica: synthesis and structure. *J. Phys. Chem. B* **2003**, *107*, 14296−14300.

(24) Bagshaw, S. A.; Prouzet, E.; Pinnavaia, T. J. Templating of mesoporous molecular sieves by nonionic polyethylene oxide surfactants. *Science* **1995**, *269*, 1242−1244.

(25) Bagshaw, S. A.; Pinnavaia, T. J. Mesoporous alumina molecular sieves. *Angew. Chem., Int. Ed.* **1996**, *35*, 1102−1105.

(26) López Pérez, L.; Perdriau, S.; Brink, G. t.; Kooi, B. J.; Heeres, H. J.; Melián-Cabrera, I. Stabilization of self-assembled alumina mesophases. *Chem. Mater.* **2013**, *25*, 848−855.

(27) López Pérez, L.; Alvarez-Galván, C.; Zarubina, V.; Figueiredo Fernandes, B. O.; Melián-Cabrera, I. A hydrothermally stable transition alumina by condensation-enhanced self-assembly and pyrolysis crystallization: application in the steam reforming of methane,. *CrystEngComm* **2014**, *16*, 6775−6783.
(28) Xu, R.; Pang, W. Q.; Yu, J. H.; Huo, Q. H.; Chen, J. H. *Chemistry of Zeolites and Related Porous Materials: Synthesis and Structure*; John Wiley & Sons: Singapore, 2007.
(29) Leng, Y.; Liu, J.; Zhang, Z.; Chen, H.; Zhang, P.; Dai, S. Polyoxometalates as bifunctional templates: engineering metal oxides with mesopores and reactive surfaces for catalysis. *J. Mater. Chem. A* **2019**, *7*, 27297−27303.
(30) Weng, Z.; Chen, Z.-h.; Qin, X.; Zaera, F. Sub-monolayer control of the growth of oxide films on mesoporous materials. *J. Mater. Chem. A* **2018**, *6*, 17548−17558.
(31) López Pérez, L.; Ortiz-Iniesta, M. J.; Jan Heeres, H.; Melián-Cabrera, I. Hot-spots during the calcination of MCM-41: A SAXS comparative analysis of a soft mesophase. *Mater. Lett.* **2014**, *118*, 51−54.
(32) *Handbook of Porous Solids*; Schüth, F.; Sing, K. S. W.; Weitkamp, J., Eds.; Wiley-VCH: Weinheim, 2002; pp 1546−1551.
(33) Zhang, Z.; Yin, J.; Heeres, H. J.; Melián-Cabrera, I. Thermal detemplation of SBA-15 mesophases. Effect of the activation protocol on the framework contraction. *Microporous Mesoporous Mater.* **2013**, *176*, 103−111.
(34) Patarin, J. Mild methods for removing organic templates from inorganic host materials. *Angew. Chem., Int. Ed.* **2004**, *43*, 3878−3880.
(35) González-Rivera, J.; Tovar-Rodríguez, J.; Bramanti, E.; Duce, C.; Longo, I.; Fratini, E.; Galindo-Esquivel, I. R.; Ferrari, C. Surfactant recovery from mesoporous metal-modified materials (Sn−, Y−, Ce−, Si−MCM-41), by ultrasound assisted ion-exchange extraction and its re-use for a microwave in situ cheap and eco-friendly MCM-41 synthesis. *J. Mater. Chem. A* **2014**, *2*, 7020−7033.
(36) Grün, M.; Unger, K. K.; Matsumoto, A.; Tsutsumi, K. Novel pathways for the preparation of mesoporous MCM-41 materials: control of porosity and morphology. *Microporous Mesoporous Mater.* **1999**, *27*, 207−216.
(37) Tian, B.; Liu, X.; Yu, C.; Gao, F.; Luo, Q.; Xie, S.; Tu, B.; Zhao, D. Microwave assisted template removal of siliceous porous materials. *Chem. Commun.* **2002**, 1186−1187.
(38) Büchel, G.; Denoyel, R.; Llewellyn, P. L.; Rouquerol, J. In situ surfactant removal from MCM-type mesostructures by ozone treatment. *J. Mater. Chem.* **2001**, *11*, 589−593.
(39) Kleitz, F.; Schmidt, W.; Schüth, F. Evolution of mesoporous materials during the calcination process: structural and chemical behavior. *Microporous Mesoporous Mater.* **2001**, *44*−*45*, 95−109.
(40) Kleitz, F.; Schmidt, W.; Schüth, F. Calcination behavior of different surfactant-templated mesostructured silica materials. *Microporous Mesoporous Mater.* **2003**, *65*, 1−29.
(41) Groen, J. C.; Pérez-Ramírez, J. Critical appraisal of mesopore characterization by adsorption analysis. *Appl. Catal. Gen.* **2004**, *268*, 121−125.
(42) Lowell, S.; Shields, J. E.; Thomas, M. A.; Thommes, M.. *Characterization of Porous Solids and Powders: Surface Area, Pore Size and Density*; Springer: Dordrecht, 2004.
(43) Fubini, B.; Bolis, V.; Cavenago, A.; Garrone, E.; Ugliengo, P. Structural and induced heterogeneity at the surface of some silica polymorphs from the enthalpy of adsorption of various molecules. *Langmuir* **1993**, *9*, 2712−2720.
(44) Majda, D.; Zimowska, M.; Tarach, K.; Góra-Marek, K.; Napruszewska, B. D.; Michalik-Zym, A. Water thermoporosimetry as a tool of characterization of the textural parameters of mesoporous materials. *J. Therm. Anal. Calorim.* **2017**, *127*, 207−220.
(45) Zhang, Z.; Santangelo, D. L.; ten Brink, G.; Kooi, B. J.; Moulijn, J. A.; Melián-Cabrera, I. On the drug adsorption capacity of SBA-15 obtained from various detemplation protocols. *Mater. Lett.* **2014**, *131*, 186−189.
(46) Lide, D. R. *CRC Handbook of Chemistry and Physics*, 89th ed.; CRC Press Taylor Francis Group: Boca Raton, 2008; pp 8−20.
(47) Tarr, M. A.. *Chemical Degradation Methods for Wastes and Pollutants: Environmental and Industrial Applications*; Marcel Dekker, Inc.: New York, 2003; p 5.
(48) Xiouras, C.; Radacsi, N.; Sturm, G.; Stefanidis, G. D. Furfural synthesis from d-xylose in the presence of sodium chloride: microwave versus conventional heating. *ChemSusChem* **2016**, *9*, 2159−2166.
(49) Priecel, P.; Lopez-Sanchez, J. A. Advantages and limitations of microwave reactors: from chemical synthesis to the catalytic valorization of biobased chemicals. *ACS Sustainable Chem. Eng.* **2019**, *7*, 3−21.
(50) Navarro, M.; Morris, S. A.; Mayoral, Á.; Čejka, J.; Morris, R. E. Microwave heating and the fast ADOR process for preparing zeolites. *J. Mater. Chem. A* **2017**, *5*, 8037−8043.

https://dx.doi.org/10.1021/acssuschemeng.0c05438
ACS Sustainable Chem. Eng. 2020, 8, 16814−16822